PHYSICAL REVIEW A **94**, 032109 (2016)

Rotation sensing using a K-Rb-^{21}Ne comagnetometer

Rujie Li,* Wenfeng Fan, Liwei Jiang, Lihong Duan, Wei Quan, and Jiancheng Fang
School of Instrument Science and Opto-Electronics Engineering, and Science and Technology on Inertial Laboratory, Beihang University, Beijing 100191, China
(Received 27 March 2016; published 8 September 2016)

We report on the Earth's rotation measurement using a K-Rb-^{21}Ne comagnetometer. The steady-state responses of the nuclear- and electronic-spin polarizations therein have been shown. The light shift arising from the circularly polarized pump laser beam enables the comagnetometer to sense dual-axis rotations. This feasibility has been emphasized and verified by numerical simulation. We believe that this sensor could be used in any application requiring compact size, low cost, and high-precision inertial navigation.

DOI: 10.1103/PhysRevA.94.032109

I. INTRODUCTION

High-precision gyroscopes have found applications in the field of general relativity test, gravitational wave detection, downhole orientation sensing, and inertial navigation [1–5]. The traditional electromechanical gyroscope developed in the 1920s has dominated the above-mentioned applications. With the development of fibers and lasers in the 1960s, the fiber optic gyroscope (FOG) and the ring laser gyroscope (RLG) replaced electromechanical devices in many applications by the late 1980s [6]. Recent technological advancements, mainly progress on quantum mechanics and modern optics, are enabling a new generation of inertial navigation sensors relying on atoms. Utilizing the Sagnac effect of laser-cooled atoms, the atom interferometer gyroscope (AIG) shows the unrivaled ultrahigh rotation sensitivity and is used to test general relativity [7,8]. The micro nuclear magnetic resonance gyroscope (micro-NMRG) developed by the Northrop Grumman Corporation in the past decade offers small size, low-power package, and near navigation-grade performance [9,10]. Also, the atomic spin gyroscope (ASG), also called the alkali-metal-noble-gas comagnetometer, operates in the spin-exchange relaxation-free (SERF) regime where spin-exchange collisions do not broaden the magnetic resonance linewidth and features a higher sensitivity than micro-NMRG [11,12]. In the ASG, the sensitivity to the magnetic fields can be effectively suppressed, but the potential to achieve ultrasensitive rotation measurements has been kept. Utilizing the microfabrication techniques first developed for chip-scale atomic clocks [13–15], the ASG has the potential to reach a much more compact size in the near future compared to the AIG.

For the ASG based on K-^{3}He, the ability to sense rotation has been demonstrated only as a single axis inertial sensor so far. By adding a second probe laser beam, the theoretical possibility of a dual-axis gyroscope has been analyzed in the our previous work [16], where we have ignored the influences arising from the light shift. Here, we report on the Earth's rotation measurement based on a K-Rb-^{21}Ne comagnetometer. By investigating the steady-state response of the nuclear- and electronic-spin polarizations, we have found that the existence of the light shift arising from the circularly polarized pump laser beam adds sensitivity to the rotation velocity along another direction. The effectiveness operated as a two-axis inertial sensor has been verified by numerical simulation. The comagnetometer presented here provides a promising tool for navigation systems demanding a portable package, low cost, and high-precision inertial sensor.

II. OPERATION PRINCIPLE

The behavior of the comagnetometer can be approximated by a set of Bloch equations that coupled the polarization of the electron $\mathbf{P}^e$ with the polarization of the nuclear $\mathbf{P}^n$ [11]:

$$\frac{\partial \mathbf{P}^e}{\partial t} = \frac{\gamma^e}{Q(P^e)}(\mathbf{B} + \lambda M^n \mathbf{P}^n + \mathbf{L}) \times \mathbf{P}^e - \Omega \times \mathbf{P}^e + \frac{\left(R_p \mathbf{s}^p + R_{se}^{en}\mathbf{P}^n + R_m \mathbf{s}^m - R_{\mathrm{tot}}^e \mathbf{P}^e\right)}{Q(P^e)}, \quad (1)$$

$$\frac{\partial \mathbf{P}^n}{\partial t} = \gamma^n(\mathbf{B} + \lambda M^e \mathbf{P}^e) \times \mathbf{P}^n - \Omega \times \mathbf{P}^n + R_{se}^{ne}(\mathbf{P}^e - \mathbf{P}^n) - R_{sd}^n \mathbf{P}^n. \quad (2)$$

The above equations are written in the rotating frame. γ^e and γ^n are the gyromagnetic ratio of the electron and the nuclear spins. Q is the slowing-down factor and is a function of the electron polarization. Each spin species precesses in the sum of the ambient magnetic field $\mathbf{B}$ and the effective field due to the polarization of the other species $\lambda M\mathbf{P}$, while M^e and M^n are the magnetizations of electron and nuclear spins corresponding to full spin polarizations. Note that the electron spin additionally presses in an ac-Stark shift (light shift) field $\mathbf{L}$, a magneticlike field arising from the pumping and probing lasers [17,18]. Ω is the rotation vector. The electron spins relax at a rate $R_{\mathrm{tot}}^e = R_p + R_m + R_{sd}^e + R_{se}^{en}$, where R_p is the pumping rate from the pump beam, R_m is the pumping rate from the probe beam, R_{sd}^e is the spin-destruction rate, and R_{se}^{en} is the spin-exchange rate experienced by the electron spins. $\mathbf{s}^p$ and $\mathbf{s}^m$ are the optical pumping vectors which define the direction and the degree of circular polarization of the pump and the probe light. The polarization of the nuclear spin is defined by the balance of the spin-exchange rate R_{se}^{ne} and the relaxation rate R_{sd}^n. As the angle of the polarization vector with respect to the z axis is small enough, it is a good approximation to assume that the longitudinal components P_z^e and P_z^n are not affected by the presence of the transverse components. Thus, it is convenient to write the Bloch equations as a system

*lirujie@buaa.edu.cn

of equations for $\tilde{P}^e = P_x^e + iP_y^e$ and $\tilde{P}^n = P_x^n + iP_y^n$ in the matrix form

$$\begin{bmatrix} \dfrac{\partial \tilde{P}^e}{\partial t} \\ \dfrac{\partial \tilde{P}^n}{\partial t} \end{bmatrix} = A \begin{bmatrix} \tilde{P}^e \\ \tilde{P}^n \end{bmatrix} + C, \tag{3}$$

where the coefficients (matrices) of A and C are defined by Eqs. (4) and (5).

$$A = \begin{bmatrix} -\frac{R_{\rm tot}^e}{Q} + i\left(-\Omega_z + \frac{\gamma^e}{Q}\left(B_z + L_z + \lambda M^n P_z^n\right)\right) & \frac{R_{se}^{en}}{Q} - i\frac{\gamma^e}{Q}\lambda M^n P_z^e \\ R_{se}^{ne} - i\gamma^n \lambda M^e P_z^n & -R_{\rm tot}^n + i\left(-\Omega_z + \gamma^n\left(B_z + \lambda M^e P_z^e\right)\right) \end{bmatrix}, \tag{4}$$

$$C = \begin{bmatrix} P_z^e\left(-\Omega_y + \frac{\gamma^e}{Q}(B_y + L_y)\right) + \frac{R_m s_x^m}{Q} - iP_z^e\left(-\Omega_x + \frac{\gamma^e}{Q}(B_x + L_x)\right) \\ P_z^n(-\Omega_y + \gamma^n B_y) - iP_z^n(-\Omega_x + \gamma^n B_x) \end{bmatrix}, \tag{5}$$

The steady-state response of the Bloch equations can be solved analytically by setting the left-hand side of Eq. (3) to zero. The equilibrium description for the real and imaging parts of the nuclear-spin polarization $\tilde{P}^n$ is expressed by Eqs. (6) and (7), while Eqs. (8) and (9) correspond to those of $\tilde{P}^e$. Due to the symmetry between x and y axes with respect to the z axis, the terms associated with x in P_x^e have been replaced by those with y in P_y^e with the same signs, while the terms associated with y in P_x^e have been replaced by those with x in P_y^e but feature opposite signs. The expression forms of P_x^e and P_y^e are almost the same except for the last term arising from the pumping effect produced by the probe beam.

$$P_x^n = \frac{P_z^n}{B_c + \delta B_z - \Omega_z/\gamma^n}\left(B_x - \frac{\Omega_x}{\gamma^n}\right), \tag{6}$$

$$P_y^n = \frac{P_z^n}{B_c + \delta B_z - \Omega_z/\gamma^n}\left(B_y - \frac{\Omega_y}{\gamma^n}\right), \tag{7}$$

$$\begin{aligned} P_x^e = {} & \frac{\gamma^e P_z^e R_{\rm tot}^e}{{R_{\rm tot}^e}^2 + (\gamma^e)^2(L_z + \delta B_z - Q\Omega_z/\gamma^e)^2} \\ & \times\Bigg[\tilde{\Omega}_y + \frac{\gamma^e}{R_{\rm tot}^e}(L_z + \delta B_z)(L_x + \tilde{\Omega}_x) + L_y + \frac{B_y + L_y}{B_c}\left(\delta B_z - \frac{\Omega_z}{\gamma^n}\right) + \frac{\gamma^e(B_x + L_x)}{R_{\rm tot}^e B_c}\left(L_z + \delta B_z - \left(\frac{1}{\gamma^n} + \frac{Q}{\gamma^e}\right)\Omega_z\right)\delta B_z \\ & + \frac{P_z^n R_{se}^{en}}{P_z^e \gamma^e}\frac{1}{B_c}\left(B_x - (L_z + \delta B_z)\left(B_y - \frac{\Omega_y}{\gamma^n}\right) - \frac{\Omega_x}{\gamma^n} + B_y\frac{Q\Omega_z}{\gamma^e} - \frac{Q\Omega_y}{\gamma^e}\frac{\Omega_z}{\gamma^n}\right) - \frac{\gamma^e \delta B_z}{R_{\rm tot}^e B_c}(L_z + \delta B_z)\frac{Q\Omega_x}{\gamma^e} \\ & - \frac{\gamma^e}{R_{\rm tot}^e}(B_x + L_x)\left(\frac{L_z}{\gamma^n B_c} + \frac{Q}{\gamma^e}\right)\Omega_z - \frac{\delta B_z}{B_c}\frac{Q\Omega_y}{\gamma^e} + \frac{\gamma^e}{R_{\rm tot}^e}B_x\frac{Q\Omega_z}{\gamma^e} + \frac{\gamma^e}{R_{\rm tot}^e}\left(\frac{L_z + \delta B_z}{B_c} - 1\right)\frac{Q\Omega_x}{\gamma^e}\frac{\Omega_z}{\gamma^n} \\ & + \frac{\gamma^e}{R_{\rm tot}^e}\left(1 + \frac{\delta B_z}{B_c}\right)\frac{Q\Omega_x}{\gamma^e}\frac{Q\Omega_z}{\gamma^e} + \frac{1}{B_c}\frac{Q\Omega_y}{\gamma^e}\frac{\Omega_z}{\gamma^n} + \frac{\gamma^e}{R_{\rm tot}^e}\left(\frac{B_x + L_x}{B_c} - \frac{1}{B_c}\frac{Q\Omega_x}{\gamma^e}\right)\frac{Q\Omega_z}{\gamma^e}\frac{\Omega_z}{\gamma^n} + \frac{R_m s_x^m}{P_z^e \gamma^e}\left(1 + \frac{\delta B_z}{B_c} - \frac{1}{B_c}\frac{\Omega_z}{\gamma^n}\right)\Bigg], \end{aligned} \tag{8}$$

$$\begin{aligned} P_y^e = {} & \frac{\gamma^e P_z^e R_{\rm tot}^e}{{R_{\rm tot}^e}^2 + (\gamma^e)^2(L_z + \delta B_z - Q\Omega_z/\gamma^e)^2} \\ & \times\Bigg[-\tilde{\Omega}_x + \frac{\gamma^e}{R_{\rm tot}^e}(L_z + \delta B_z)(L_y + \tilde{\Omega}_y) - L_x - \frac{B_x + L_x}{B_c}\left(\delta B_z - \frac{\Omega_z}{\gamma^n}\right) + \frac{\gamma^e(B_y + L_y)}{R_{\rm tot}^e B_c}\left(L_z + \delta B_z - \left(\frac{1}{\gamma^n} + \frac{Q}{\gamma^e}\right)\Omega_z\right)\delta B_z \\ & + \frac{P_z^n R_{se}^{en}}{P_z^e \gamma^e}\frac{1}{B_c}\left(B_y + (L_z + \delta B_z)\left(B_x - \frac{\Omega_x}{\gamma^n}\right) - \frac{\Omega_y}{\gamma^n} - B_x\frac{Q\Omega_z}{\gamma^e} + \frac{Q\Omega_x}{\gamma^e}\frac{\Omega_z}{\gamma^n}\right) - \frac{\gamma^e \delta B_z}{R_{\rm tot}^e B_c}(L_z + \delta B_z)\frac{Q\Omega_y}{\gamma^e} \\ & - \frac{\gamma^e}{R_{\rm tot}^e}(B_y + L_y)\left(\frac{L_z}{\gamma^n B_c} + \frac{Q}{\gamma^e}\right)\Omega_z + \frac{\delta B_z}{B_c}\frac{Q\Omega_x}{\gamma^e} + \frac{\gamma^e}{R_{\rm tot}^e}B_y\frac{Q\Omega_z}{\gamma^e} + \frac{\gamma^e}{R_{\rm tot}^e}\left(\frac{L_z + \delta B_z}{B_c} - 1\right)\frac{Q\Omega_y}{\gamma^e}\frac{\Omega_z}{\gamma^n} \\ & + \frac{\gamma^e}{R_{\rm tot}^e}\left(1 + \frac{\delta B_z}{B_c}\right)\frac{Q\Omega_y}{\gamma^e}\frac{Q\Omega_z}{\gamma^e} - \frac{1}{B_c}\frac{Q\Omega_x}{\gamma^e}\frac{\Omega_z}{\gamma^n} + \frac{\gamma^e}{R_{\rm tot}^e}\left(\frac{B_y + L_y}{B_c} - \frac{1}{B_c}\frac{Q\Omega_y}{\gamma^e}\right)\frac{Q\Omega_z}{\gamma^e}\frac{\Omega_z}{\gamma^n} \\ & + \frac{R_m s_x^m}{P_z^e \gamma^e}\left(L_z + \delta B_z + \frac{\delta B_z}{B_c}\left(L_z + \delta B_z - \left(\frac{1}{\gamma^n} + \frac{Q}{\gamma^e}\right)\Omega_z\right) - \frac{L_z}{B_c}\frac{\Omega_z}{\gamma^n} - \frac{Q}{\gamma^e}\left(1 - \frac{1}{B_c}\frac{\Omega_z}{\gamma^n}\right)\Omega_z\right)\Bigg] \end{aligned} \tag{9}$$

An external compensation field B_c is employed in the comagnetometer to cancel the magnetization generated by the nuclear- and electron-spin polarization. The compensation field B_c is defined by

$$B_c = -\lambda M^n P_z^n - \lambda M^e P_z^e \approx -\lambda M^n P_z^n, \tag{10}$$

where $\lambda = 8\pi\kappa_0/3$ is the geometrical factor containing the enhancement factor [19,20]. The total residual field sensed by the electron spins along the z direction, δB_z, is defined as

$$\delta B_z = B_z + \lambda M^n P_z^n, \tag{11}$$

where the ambient magnetic field B_z (z component of **B**) is the sum of B_c and B_r, and B_r indicates the residual magnetic field of the magnetic shields. As B_r is small and much less than B_c, the total residual field δB_z approaches zero at the compensation point ($\delta B_z \approx B_c + \lambda M^n P_z^n \approx 0$). This is also the key to put the alkali-metal atoms in the SERF regime. Since $\delta B_z, \Omega_z/\gamma^n \ll B_c$, Eqs. (6) and (7) can be simplified to

$$P_x^n \approx \frac{P_z^n}{B_c}\left(B_x - \frac{\Omega_x}{\gamma^n}\right), \tag{12}$$

$$P_y^n \approx \frac{P_z^n}{B_c}\left(B_y - \frac{\Omega_y}{\gamma^n}\right), \tag{13}$$

and the leading terms of Eqs. (8) and (9) can be written as

$$P_x^e \approx \frac{\gamma^e P_z^e R_{\rm tot}^e}{{R_{\rm tot}^e}^2 + (\gamma^e)^2(L_z + \delta B_z - Q\Omega_z/\gamma^e)^2}\left[\tilde{\Omega}_y + \frac{\gamma^e}{R_{\rm tot}^e}(L_z + \delta B_z)\tilde{\Omega}_x + \frac{\gamma^e}{R_{\rm tot}^e}(L_z + \delta B_z)L_x + \frac{\gamma^e(B_x + L_x)}{R_{\rm tot}^e B_c}(L_z + \delta B_z)\delta B_z + L_y + \frac{B_y + L_y}{B_c}\delta B_z + \frac{R_m s_x^m}{P_z^e \gamma^e}\right], \tag{14}$$

$$P_y^e \approx \frac{\gamma^e P_z^e R_{\rm tot}^e}{{R_{\rm tot}^e}^2 + (\gamma^e)^2(L_z + \delta B_z - Q\Omega_z/\gamma^e)^2}\left[-\tilde{\Omega}_x + \frac{\gamma^e}{R_{\rm tot}^e}(L_z + \delta B_z)\tilde{\Omega}_y + \frac{\gamma^e}{R_{\rm tot}^e}(L_z + \delta B_z)L_y + \frac{\gamma^e(B_y + L_y)}{R_{\rm tot}^e B_c}(L_z + \delta B_z)\delta B_z - L_x - \frac{B_x + L_x}{B_c}\delta B_z + \frac{R_m s_x^m}{P_z^e \gamma^e}(L_z + \delta B_z)\right], \tag{15}$$

where $\tilde{\Omega} = (1/\gamma^n - Q/\gamma^e)\Omega$.

The response of the SERF magnetometer is given by [12,21]

$$P_x^e \approx \frac{\gamma^e P_z^e}{R_{\rm tot}^e} B_y. \tag{16}$$

Note that the leading term B_y of the SERF magnetometer described by Eq. (16) will not be the primary term of Eq. (14). This means that in the comagnetometer the sensitivity to the external magnetic fields has been effectively suppressed while the sensitivity to the inertial rotation velocity has been retained. Under the condition that $L_z \approx 0$, the comagnetometer is much more sensitive to the rotation about the y axis, Ω_y, as apposed to the other directions [11]. Compared to our previous result [22], here the analysis emphasizes the condition where L_z has not been ignored, while the terms associated with Ω_x and Ω_z have also been taken into account. In order to estimate the significance of each term in Eq. (14), the typical experimental value of each parameter has been assigned, and the corresponding magnitude has been estimated and included in Table I. As listed in Table I, the magnitude of the second term, arising from the cross-talk effect due to the nonzero light shift L_z, is comparable to the initial sensitive term (the first term). This enables the comagnetometer to obtain the extra sensitivity to the x-axis rotation velocity Ω_x.

III. EXPERIMENTAL APPARATUS

Figure 1 shows the diagram of the comagnetometer sensor head operated in the spin-exchange relaxation-free regime [12]. Here a 10-mm-diameter spherical vapor cell containing a mixture of K and Rb alkali metals, 50 torr of N_2 gas to quench the excited state of alkali-metal atoms, and 2.3 amagat (amg) of ^{21}Ne gas is used. The cell is held in an oven heated with twisted-pair wires. The density ratio of K to Rb atoms is about 1:50 at 180 °C. The cell is enclosed by four cylindrical layers made from high μ-metal magnetic shields, which provide a shielding factor of 10^6 to quasistatic magnetic fields. The residual magnetic fields can be further canceled actively by a set of three orthogonal Helmholtz coils inside the shields [23].

A circularly polarized pump beam, formed by an external cavity diode laser and turned on the K D_1 resonance line at 770.1 nm, propagates through the cell center. The K atoms are spin polarized along the z-axis direction by the pump laser beam. Rapid spin-exchange collisions between the K and Rb atoms transfer the K polarization to the Rb

TABLE I. Magnitude estimation of the leading terms in the steady-state response described by Eq. (14). Note that the common factor therein has not been shown to facilitate the analysis.

Leading term	Magnitude
$\tilde{\Omega}_y$	1.47×10^{-4}
$\frac{\gamma^e}{R_{\rm tot}^e}(L_z + \delta B_z)\tilde{\Omega}_x$	9.17×10^{-5}
$\frac{\gamma^e}{R_{\rm tot}^e}(L_z + \delta B_z)L_x$	4.82×10^{-4}
$\frac{\gamma^e(B_x+L_x)}{R_{\rm tot}^e B_c}(L_z + \delta B_z)\delta B_z$	-2.04×10^{-6}
L_y	7.74×10^{-4}
$\frac{B_y+L_y}{B_c}\delta B_z$	-3.27×10^{-6}
$\frac{R_m s_x^m}{P_z^e \gamma^e}$	5.81×10^{-7}
Other high-order terms	$<10^{-7}$

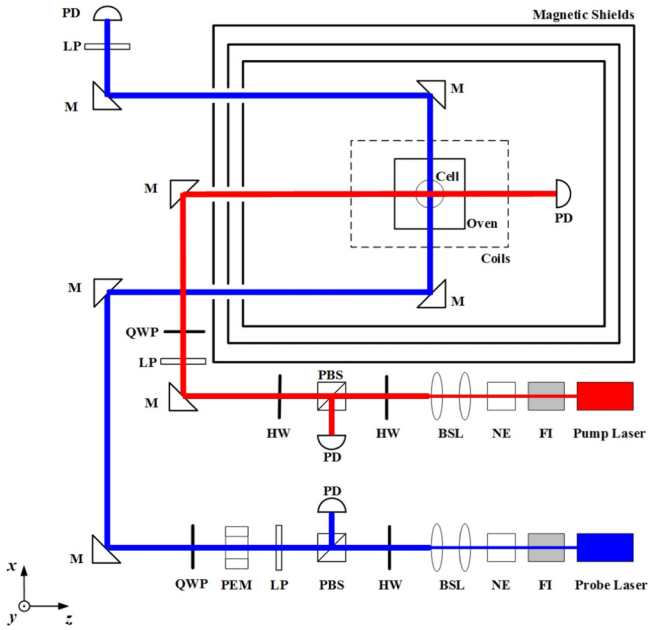

FIG. 1. Diagram of the K-Rb-^{21}Ne comagnetometer sensor head. The outer dimension of the sensor head is $350 \times 325 \times 250$ mm^3. An external controlling system outside the sensor head (not shown) is used for data processing. FI, Faraday isolator; NE, noise eater; BSL, beam shaping lenses; HW, half waveplate; PBS, polarizing beam splitter; PD, silicon photodiode; BS, beam splitter; PEM, photoelastic modulator; LP, linear polarizer; QWP, quarter waveplate; M, reflection mirror. The pump beam, marked as red lines, is circularly polarized in order to polarize the atoms, while the off-resonant probe beam, indicated by blue lines, is designed to monitor the precession of the atomic spins.

atoms with little loss, and this is the essential part of hybrid optical pumping [24]. Finally, ^{21}Ne atoms are polarized by the spin-exchange optical pumping, relying on the weak hyperfine coupling between the Rb electron and the ^{21}Ne nucleus [25]. The spin-aligned nuclear magnetic moments of the noble gases create a net magnetic field (λM^n) of up to hundreds of nT within the vapor cell.

As described by Eqs. (12)–(15), an inertial rotation of the comagnetometer leads to the precession of the nuclear- and electron-spin polarizations. The precession can be detected by the linearly polarized probe beam. The probe beam, created by a distributed feedback laser system and propagated in the x axis at the center of the cell, is detuned by about 0.3 nm to the red side of the D_2 resonance line to detect the x component of the Rb spin polarization. The power of the probe beam is set to 2 mW. The quarter waveplate and the photoelastic modulator (PEM) are oriented at 0 and 45° with respect to the transmission axis of the polarizer. The final polarizer acts as an analyzer at 90°. The PEM is used to modulate the polarization of the probe beam and features a resonance frequency of $f = 84$ kHz and a modulation amplitude of $\alpha = 0.08$ rad. The off-resonant linearly polarized probe beam orthogonal to the optical pumping direction continuously measures the projection of the Rb spins along its propagation axis through optical rotation of the linearly polarized light.

IV. RESULTS

A simulation of the nuclear- and electron-spin response as a function of the rotation velocity with respect to the inertial frame is shown in Fig. 2. A sinusoidal variation of Ω_y, the amplitude of which is comparable to the projection of the Earth's rotation in the horizontal plane (the latitude of Beijing is about 40°), will induce a reaction of the nuclear-spin polarization along the y-axis P_y^n, while the x component P_x^n will keep stationary. According to Eq. (13), the projection component P_y^n due to Ω_y introduces an equivalent magnetic field (Ω_y/γ^n) along the y direction, which will lead to the reaction of the SERF magnetometer by Eq. (16). Note that the contribution from the field fluctuation of the external environment B_y has been compensated by the projected field of the polarized nuclear spins. For the comagnetometer based on K-^{3}He where the light shift is ignorable, only the x component of the electron-spin polarization P_x^e will give a response. However, the existence of the light shift will make P_y^e sensitive

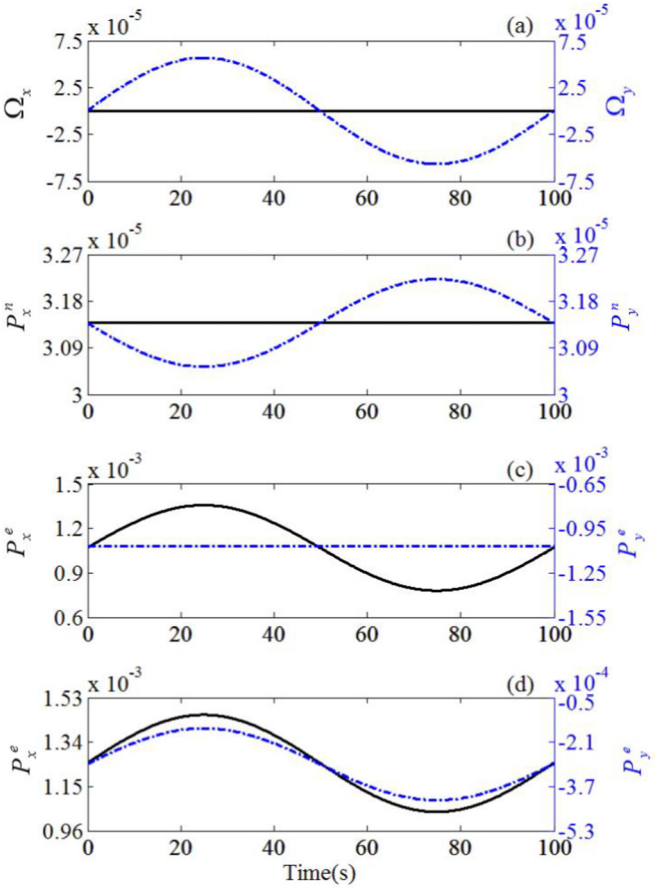

FIG. 2. The nuclear- and electron-spin response as a function of the Earth's rotation. (a) The sinusoidal variation of Ω_y is the projection of the earth rotation and could be generated by rotating the heading of the comagnetometer, while Ω_x is set to be zero. (b) Response of the nuclear-spin P_x^n (black line) and P_y^n (blue dot-dashed line) as a function of rotation velocity Ω_y. (c) Response of the electron-spin P_x^e (black line) and P_y^e (blue dot-dashed line) as a function of rotation velocity Ω_y with the light shift $L_z = 0$. (d) The same as (c) while $L_z = 3.0$ nT.

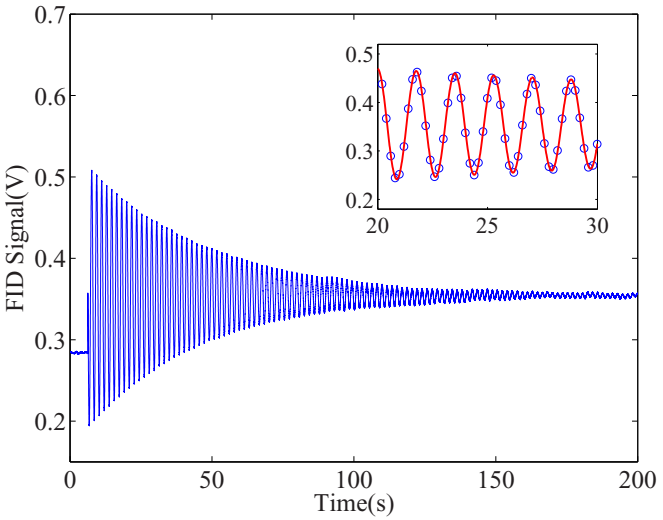

FIG. 3. A sample of the FID signals of the nuclear-spin polarization of ^{21}Ne. The inset shows the magnification of the data in the period of 20–30 s, and the fitting curve (red line) gives a precession frequency of 0.689 Hz. This Larmor precession frequency agrees very well with the value calculated by $f = \gamma^n B/(2\pi)$ based on the magnetic field $B_z = 210$ nT.

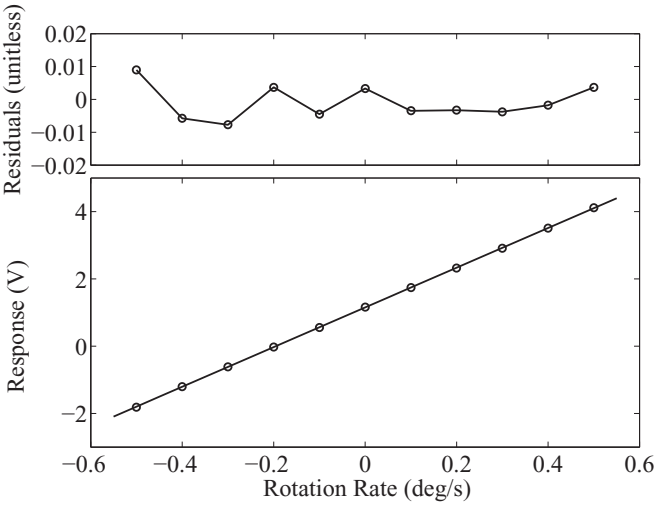

FIG. 5. The response of the comagnetometer and the corresponding residuals as a function of the rotation rate in the range of -0.5 to $+0.5$ deg/s. The linear fitting curve gives a scale factor of 5.9 V/(deg/s) and the parameters of the fit have a statistical fitting error less than 1.0% for the present apparatus.

to Ω_y and also show a response according to Eq. (15), shown in Fig. 2.

During the optical pumping process, a holding longitudinal magnetic field is employed along the pump laser direction (z axis) to facilitate the polarization of noble gas ^{21}Ne. As shown in Fig. 3, a sample of the free-induction-decay (FID) signals has been recorded to monitor the polarization of ^{21}Ne [27]. The Larmor frequency of 0.689 Hz for the ^{21}Ne in Fig. 3 corresponds to a holding field of about 205 nT, and the result agrees very well with the applied field B_z within the error due to the residual magnetic field of the magnetic shields. The longitudinal polarization of ^{21}Ne is shown in Fig. 4 and

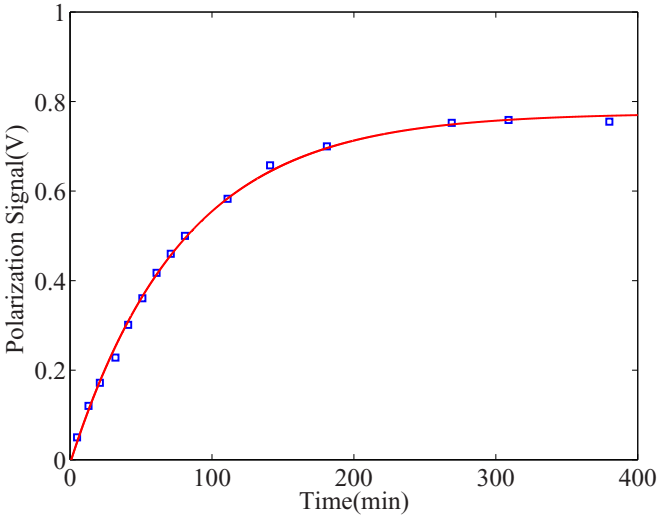

FIG. 4. T_1 time measurement of the longitudinal nuclear-spin polarization of ^{21}Ne. The fitting curve (red line) indicates that T_1 is about 79 min with a cell temperature of 180 °C.

a T_1 time of 79 min is deduced with a cell temperature of 180 °C, and the longitudinal relaxation time is consistent with the work by Ghosh and Romalis [28].

After the polarization reaches the equilibrium state, the holding field slowly and smoothly decreases to find the compensation point according to Eq. (10). Thus the comagnetometer obtains the ability to sense the inertial rotation. The comagnetometer sensor head was placed on a rotary platform and its response to input rotation rate varying from -0.5 to $+0.5$ deg/s has been tested. A figure illustrating the linearity of the scale factor and the corresponding residuals is shown in Fig. 5. A sensitivity of 4.6×10^{-7} (rad/s)/Hz$^{1/2}$ for a K-Rb-^{21}Ne comagnetometer has been reported in our previous work [26], and a bias drift of 0.1 deg/h has been obtained here.

To sense the Earth's rotation, the probe beam (x direction) is mounted vertically and thus the sensitive y axis of the comagnetometer is oriented in the horizontal plane. The rotations around the vertical x axis reorient the apparatus, and the projection of the Earth's rotation on the y axis with a sinusoidal variation will be introduced into the sensor. After accomplishing each heading angle rotation, the comagnetometer will be laid stationary for a while before its output signal is collected by the data acquisition card under the Labview environment. The y axis of the comagnetometer is initially aligned with the west-east direction and the overall system response as a function of the heading angle is illuminated in Fig. 6. The fitting curve features a phase shift of 12 deg, which we suspect is due to the residual cross talk from Ω_x. The maximal value will be achieved when the y axis is aligned along the north-south position, where the projected rotation velocity reaches the maximum, and the center of the curve corresponds to the west-east direction. The result demonstrates that the comagnetometer based on K-Rb-^{21}Ne is capable of detecting the y-axis rotation velocity Ω_y.

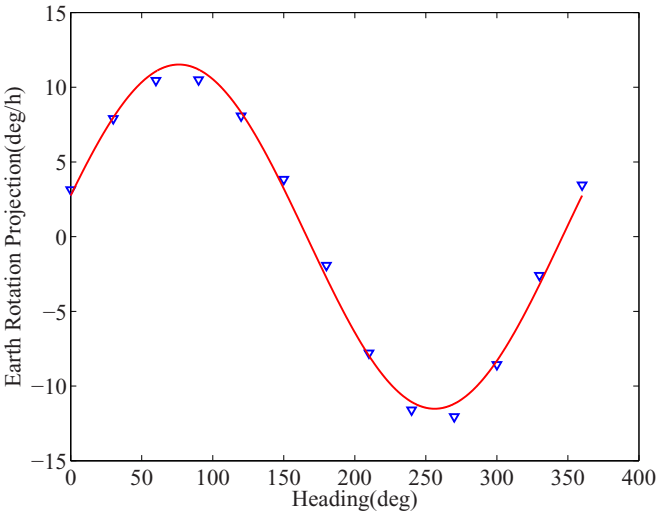

FIG. 6. The gyroscope response to Ω_y from the Earth's rotation. The rotations of the sensor about the x axis reorient the direction of the y axis with respect to the celestial frame, and the projection of the Earth's rotation with a sinusoidal variation will be introduced into Ω_y while Ω_x is kept as a constant. The fitting curve (red line) overlapping the data points gives an initial phase of about 12 deg.

V. CONCLUSION AND FUTURE WORK

In summary, here we investigate the steady-state response of the nuclear- and electron-spin polarization of the comagnetometer operated in the SERF regime, and study the feasibility of inertial rotation measurements based on K-Rb-^{21}Ne. This work will be helpful to understand the operation principle of the comagnetometer. The comagnetometer response to the projection of the Earth's rotation on the y axis has been collected and analyzed. Except for the y-axis sensitivity reported by Kornack *et al.* [11], in this paper we have shown that the x axis will also become the sensitive axis due to the nonzero value of light shift L_z in the hybrid optical pumping systems.

The inertial device operated in the SERF regime is arguably simpler, more robust, and more compact than atom interferometer sensors published so far. It is also capable of competing with FOG or RLG on both precision and price. As the inertial measurement based on the comagnetometer relies on the Larmor precession of the nuclear spins, we estimate that the bandwidth of the comagnetometer is less than that of the FOG or RLG. From our perspective, the SERF comagnetometer presented here is especially ideal for high-precision inertial navigation systems demanding a portable package, low cost, and low power, but not necessarily high bandwidth.

We also identify further improvements. A lighter physical package and better performance could benefit from structure revolution, which might be achieved by utilizing compact optics with microelectromechanical systems (MEMS) fabrication and the advances in electronics developed for chip-scale atomic clocks [13–15]. The cross-talk effects between the two sensitive axes contained in P_x^e will limit its future application. The corresponding decoupling method is being investigated and will be published in our future work.

ACKNOWLEDGMENTS

This work is supported by the National Natural Science Foundation of China (Grant No. 61227902), the National Key R&D Program of China (Grant No. 2016YFB0501601), and the Academic Excellence Foundation of Beihang University (BUAA) for PhD Students.

[1] C. W. F. Everitt, D. B. DeBra, B. W. Parkinson, J. P. Turneaure, J. W. Conklin, M. I. Heifetz, G. M. Keiser, A. S. Silbergleit, T. Holmes, J. Kolodziejczak, M. Al-Meshari, J. C. Mester, B. Muhlfelder, V. G. Solomonik, K. Stahl, P. W. Worden, W. Bencze, S. Buchman, B. Clarke, A. Al-Jadaan, H. Al-Jibreen, J. Li, J. A. Lipa, J. M. Lockhart, B. Al-Suwaidan, M. Taber, and S. Wang, Phys. Rev. Lett. **106**, 221101 (2011).
[2] M. S. Shahriar and M. Salit, J. Mod. Opt. **55**, 3133 (2008).
[3] G. E. Stedman, Rep. Prog. Phys. **60**, 615 (1997).
[4] E. M. Samson, J. L. Maida, and J. Luscombe, US Patent No. 8278923 (2012).
[5] W. W. Chow, J. Gea-Banacloche, L. M. Pedrotti, V. E. Sanders, W. Schleich, and M. O. Scully, Rev. Mod. Phys. **57**, 61 (1985).
[6] S. J. Sanders, L. K. Strandjord, and D. Mead, in *Proceedings of 15th Optical Fiber Sensors Conference Technical Digest* (IEEE, Portland, OR, 2002), pp. 5–8.
[7] T. L. Gustavson, A. Landragin, and M. A. Kasevich, Classical Quantum Gravity **17**, 2385 (2000).
[8] S. Dimopoulos, P. W. Graham, J. M. Hogan, and M. A. Kasevich, Phys. Rev. Lett. **98**, 111102 (2007).
[9] E. A. Donley, in *Proceedings of IEEE Sensors* (IEEE, Kona, HI, 2010), pp. 17–22.
[10] M. Larsen and M. Bulatowicz, in *Proceedings of International Symposium on Inertial Sensors and Systems (ISISS)* (IEEE, Laguna Beach, CA, 2014), pp. 1–5.
[11] T. W. Kornack, R. K. Ghosh, and M. V. Romalis, Phys. Rev. Lett. **95**, 230801 (2005).
[12] J. Fang, R. Li, L. Duan, Y. Chen, and W. Quan, Rev. Sci. Instrum. **86**, 073116 (2015).
[13] S. Knappe, V. Shah, P. D. D. Schwindt, L. Hollberg, J. Kitching, L.-A. Liew, and J. Moreland, Appl. Phys. Lett. **85**, 1460 (2004).
[14] S. Knappe, P. D. D. Schwindt, V. Shah, L. Hollberg, J. Kitching, L. Liew, and J. Moreland, Opt. Express **13**, 1249 (2005).
[15] R. Straessle, M. Pellaton, C. Affolderbach, Y. Pétremand, D. Briand, G. Mileti, and N. F. de Rooij, Appl. Phys. Lett. **105**, 043502 (2014).
[16] J. Qin, J. Fang, and S. Wan, in *Proceedings of Eighth IEEE International Symposium on Instrumentation and Control Technology (ISICT)* (IEEE, London, 2012), pp. 24–27.
[17] B. S. Mathur, H. Tang, and W. Happer, Phys. Rev. **171**, 11 (1968).
[18] I. A. Sulai, R. Wyllie, M. Kauer, G. S. Smetana, R. T. Wakai, and T. G. Walker, Opt. Lett. **38**, 974 (2013).
[19] B. C. Grover, Phys. Rev. Lett. **40**, 391 (1978).

[20] S. R. Schaefer, G. D. Cates, T.-R. Chien, D. Gonatas, W. Happer, and T. G. Walker, Phys. Rev. A **39**, 5613 (1989).
[21] T. W. Kornack, Ph.D thesis, Princeton University, 2005.
[22] J. Fang, S. Wan, and H. Yuan, Appl. Opt. **52**, 7220 (2013).
[23] J. Fang and J. Qin, Rev. Sci. Instrum. **83**, 103104 (2012).
[24] E. Babcock, I. Nelson, S. Kadlecek, B. Driehuys, L. W. Anderson, F. W. Hersman, and T. G. Walker, Phys. Rev. Lett. **91**, 123003 (2003).
[25] T. G. Walker and W. Happer, Rev. Mod. Phys. **69**, 629 (1997).
[26] J. Fang, Y. Chen, S. Zou, X. Liu, Z. Hu, W. Quan, H. Yuan, and M. Ding, J. Phys. B **49**, 065006 (2016).
[27] S. I. Kanorsky, S. Lang, S. Lücke, S. B. Ross, T. W. Hänsch, and A. Weis, Phys. Rev. A **54**, R1010 (1996).
[28] R. K. Ghosh and M. V. Romalis, Phys. Rev. A **81**, 043415 (2010).